Unimolecular reaction of acetone oxide and its reaction with water in the atmosphere

Bo Long[a,b,c,1], Junwei Lucas Bao[b,c], and Donald G. Truhlar[b,c,1]

[a]College of Materials Science and Engineering, Guizhou Minzu University, 550025 Guiyang, China; [b]Department of Chemistry, Chemical Theory Center, University of Minnesota, Minneapolis, MN 55455-0431; and [c]Supercomputing Institute, University of Minnesota, Minneapolis, MN 55455-0431

Contributed by Donald G. Truhlar, May 3, 2018 (sent for review March 14, 2018; reviewed by William H. Green and Craig A. Taatjes)

Criegee intermediates (i.e., carbonyl oxides with two radical sites) are known to be important atmospheric reagents; however, our knowledge of their reaction kinetics is still limited. Although experimental methods have been developed to directly measure the reaction rate constants of stabilized Criegee intermediates, the experimental results cover limited temperature ranges and do not completely agree well with one another. Here we investigate the unimolecular reaction of acetone oxide [$(CH_3)_2COO$] and its bimolecular reaction with H_2O to obtain rate constants with quantitative accuracy comparable to experimental accuracy. We do this by using CCSDT(Q)/CBS//CCSD(T)-F12a/DZ-F12 benchmark results to select and validate exchange-correlation functionals, which are then used for direct dynamics calculations by variational transition state theory with small-curvature tunneling and torsional and high-frequency anharmonicity. We find that tunneling is very significant in the unimolecular reaction of $(CH_3)_2COO$ and its bimolecular reaction with H_2O. We show that the atmospheric lifetimes of $(CH_3)_2COO$ depend on temperature and that the unimolecular reaction of $(CH_3)_2COO$ is the dominant decay mode above 240 K, while the $(CH_3)_2COO + SO_2$ reaction can compete with the corresponding unimolecular reaction below 240 K when the SO_2 concentration is 9×10^{10} molecules per cubic centimeter. We also find that experimental results may not be sufficiently accurate for the unimolecular reaction of $(CH_3)_2COO$ above 310 K. Not only does the present investigation provide insights into the decay of $(CH_3)_2COO$ in the atmosphere, but it also provides an illustration of how to use theoretical methods to predict quantitative rate constants of medium-sized Criegee intermediates.

atmospheric chemistry | CCSDT(Q)/CBS | density functional theory | direct dynamics | kinetics

Criegee intermediates (1) are produced in the ozonolysis of unsaturated hydrocarbons in the atmosphere, and understanding their kinetics is important for understanding reaction mechanisms involving OH radical, sulfuric acid, secondary organic aerosols, and a variety of pollutants such as carboxylic acids and aldehydes (2–10). Stabilized Criegee intermediates undergo unimolecular decomposition reactions, bimolecular association, insertion, and addition reactions, and bimolecular reactions with water, water dimer, sulfur dioxide, atmospheric acids, HO_2, H_2O_2, aldehydes, carbon dioxide, H_2S, peroxy radicals, aldehydes, and self-reactions (2, 7–27). While the reaction kinetics of the simplest Criegee intermediate (CH_2OO) have, by now, been extensively investigated by both experimental and theoretical methods [experimental measurements have shown that the simplest Criegee intermediate mainly reacts with water dimer under some atmospheric conditions (10)], information about the bimolecular and unimolecular reaction kinetics of medium and large Criegee intermediates is still limited (7, 28).

Acetone oxide [$(CH_3)_2COO$] is produced in the ozonolysis of 2,3-dimethyl-2-butene (13, 29–31). In the present report, we focus on the unimolecular reaction of $(CH_3)_2COO$ and on its reaction with H_2O. In particular, we investigate the unimolecular hydrogen shift (**Uhs**) reaction, the unimolecular cyclization (**Uc**) reaction, the bimolecular addition (**Ba**) of water, and the bimolecular double hydrogen transfer (**Bdhs**) reaction catalyzed by H_2O,

$$CH_3(CH_3)COO \rightarrow CH_2{=}C(CH_3)OOH \ (\mathbf{Uhs})$$

$$(CH_3)_2COO \rightarrow \ ^{(CH_3)_2C}\!\!<\!\!^{O}_{O} \ (\mathbf{Uc})$$

$$(CH_3)_2COO + H_2O \rightarrow (CH_3)_2C(OH)OOH \ (\mathbf{Ba})$$

$$(CH_3)_2COO + H_2O \rightarrow CH_2{=}C(CH_3)OOH + H_2O \ (\mathbf{Bdhs})$$

Although the **Uhs** reaction of $(CH_3)_2COO$ has been extensively studied by both experimental and theoretical methods (13, 14, 29, 32–38), the results are not fully consistent with one another. The reaction with water has also been studied experimentally (22) and theoretically (39, 40).

The rate constant of the unimolecular reaction of $(CH_3)_2COO$ was directly measured to be 361 ± 49 s^{-1} at 298 K by Smith et al. (34) and 305 ± 70 s^{-1} at 293 K by Chhantyal-Pun et al. (35), but it was indirectly measured to be 3.0 ± 0.4 s^{-1} at 293 K by Berndt et al. (13), 6.4 ± 0.9 s^{-1} at an unspecified temperature (but, based on other work by this group, probably 298 K) by Kroll et al. (29), 832 ± 202 s^{-1} at 298 K by Newland et al. (32), and 643 ± 78 s^{-1} at 293 K by Berndt et al. (15). The experiments of Smith et al. (34) showed that the unimolecular reaction of $(CH_3)_2COO$ is independent of pressure over the range 100 Torr to 200 Torr at 298 K. Fang et al. (33) calculated that the unimolecular rate constant is within 10% of the high-pressure limit at 0.01 bar and 300 K and within 0.5% at 1 bar.

Significance

Obtaining rate constants and tropospheric lifetimes of Criegee intermediates is of critical significance for atmospheric modeling. We report calculations that can produce quantitative rate constants by variational transition state theory with corner-cutting tunneling based on implicit potential energy surfaces calibrated against high-level calculations. Demonstration of this capability is particularly significant because the calculations can fully cover the atmospheric conditions, which is hard to do by experiment. The present results also show the usefulness of the M11-L and MN15-L density functionals in describing this nominally multireference system. Modern quantum chemistry is now accurate enough to be used for atmospheric chemistry, and the present methods and strategies can be also be used to study other atmospherically important reactions of other medium-sized molecules.

Author contributions: B.L., J.L.B., and D.G.T. designed research, performed research, analyzed data, and wrote the paper.

Reviewers: W.H.G., Massachusetts Institute of Technology; and C.A.T., Sandia National Laboratories.

The authors declare no conflict of interest.

[1]To whom correspondence may be addressed. Email: bolong2008@gmail.com or truhlar@umn.edu.

This article contains supporting information online at www.pnas.org/lookup/suppl/doi:10.1073/pnas.1804453115/-/DCSupplemental.

For the $(CH_3)_2COO + H_2O$ reaction rate constant (sum of **Ba** and **Bhs**), experimental studies only led to an upper limit estimate, which is 1.5×10^{-16} cm^3 per molecule per second at 298 K (22).

Theoretically, the prediction of the rate constants is hard because Criegee intermediates have inherently multiconfigurational (and hence strongly correlated) electronic structures (acetone oxide is biradicaloid with radical character at the central carbon and terminal oxygen). In our previous investigations (41) of the reactions of CH_2OO and *syn*/*anti*-CH_3CHOO, which used electronic structure protocols developed by Chan and Radom (42), our best estimates for the CCSD(T) barrier heights differed from our best estimates of the CCSDT(Q) barrier heights by 0.50 kcal/mol to 0.63 kcal/mol, which would lead to errors in calculated rates of a factor of about 2.3 to 2.9 at 283 K, increasing to 3.5 to 4.9 at 200 K. (Table 1 contains explanations and references for all theoretical acronyms and basis sets used in this paper.) For the unimolecular reaction of $(CH_3)_2COO$ to produce $CH_2{=}C(CH_3)OOH$, the difference between CCSD(T) and CCCSDT(Q) was estimated by Fang et al. (33) to be 0.39 kcal/mol, corresponding to factors of about 2.7 and 1.9 in rate constants at 200 and 298 K, respectively. We conclude from these studies (33, 41) that the strongly correlated character of carbonyl oxides has the consequence that one must use higher levels of coupled cluster theory than CCSD(T) to obtain quantitative rate constants, and we will do so in the present work.

Fang et al. (33) calculated rate constants for the **Uhs** reaction with the CCSDT(Q) barrier by conventional transition state theory with Eckart tunneling (TST/E). For the **Ba** reaction, the conventional-transition-state-theory enthalpy of activation at 0 K, denoted here as $\Delta H_0^{\ddagger}$, was calculated to be 3.57 kcal/mol by CCSD(T)/aTZ//B3LYP/MG3S (40) and 4.0 kcal/mol by CCSD(T)/F84//B3LYP/F84 (39). Anglada et al. (40) calculated rate constants for the **Ba** reaction by TST/E and by canonical variational transition state theory (43) (CVT) with corner-cutting tunneling included by the small-curvature tunneling (44) (SCT) approximation.

For the work reported here, we first carry out CCSDT(Q)/CBS benchmark calculations. Then we use these benchmarks to select and validate density functionals. These tests identify and validate the M11-L and MN15-L density functionals as the methods of choice for direct dynamics calculations of the rate constants, and we use these density functionals to carry out such dynamics calculations. [Direct dynamics calculations are calculations in which "instead of using a pre-defined potential energy function, all required energies and forces for each geometry that is important for evaluating dynamical properties are obtained directly from electronic structure calculations" (45); in this way, the potential energy function is defined implicitly by the electronic structure method.]

The rate constants are calculated by multistructural variational transition state theory (46) with multistructural torsional anharmonicity (47, 48), a scale-factor treatment (49) of anharmonicity for other modes (*SI Appendix*, Table S2), and the SCT approximation for tunneling. Variational transition state theory is more reliable than conventional transition state theory, and the SCT approximation is more reliable than Eckart tunneling (50–52). We use a dual-level strategy (41) that combines our highest-level estimate of the rate constants by conventional transition state theory with variational-transition-state and tunneling effects calculated by the validated density functional. Further details are in *Computational Methods* and *SI Appendix*.

The present work not only provides quantitative rate constants for these reactions to estimate atmospheric lifetimes of $(CH_3)_2COO$, but it also shows that theoretical methods can produce quantitative

Table 1. Abbreviations for theoretical methods and basis sets

Abbreviation	Ref.	Explanation
Wave function methods		
QCISD	64	Quadratic configuration interaction with single and double excitations
QCISD(T)	64	QCISD with noniterative triple excitations
CCSD(T)	65	Coupled cluster theory with single and double excitations and noniterative triple excitations
CCSD(T)-F12a	66	CCSD(T) with simplified explicit correlation
CCSDT(Q)	67	Coupled cluster theory with single, double, and triple excitations and noniterative quadruple excitations
W2X	42	Cost-effective approximation to CCSD(T)/CBS
MW2-F12	68	Cost-effective approximation to CCSD(T)/CBS with larger basis sets
W3X	69	Cost-effective approximation to CCSDT(Q)/CBS
W3X-L	42	W3X with larger basis sets
Density functionals		
B3LYP	70	Becke three-parameter Lee–Yang–Parr
M11-L	71	Minnesota 2011 local
MN15-L	72	Minnesota Nonseparable 2015 local
Basis sets		
F84	73	6-311++G(2d,2p)
MG3S	74	Modified G3 semidiffuse; same as 6-311+G(2df,2p) for H, C, and O
DZ-F12	75	cc-pVDZ-F12
TZ	76	cc-pVTZ
mTZ	77	maug-cc-pVTZ
aTZ	78	aug-cc-pVTZ
CBS	79	Complete basis set (limit obtained by extrapolation)
Kinetics methods		
TST/E	80	Conventional transition state theory with Eckart tunneling
CVT	43	Canonical variational transition stat theory
MS-VTST	46	Multistructural variational transition stat theory
SCT	44	Small-curvature tunneling

We use the standard notation by which A/B denotes geometries and energies calculated by method A and basis set B, and A/B//C/D denotes single-point energies by A/B at geometries optimized by C/D. W3X-L//CCSD(T)-F12a/DZ-F12 denotes that the geometrical optimizations and frequency calculations were done by CCSD(T)-F12a/DZ-F12 and single-point energy calculations were done using W3X-L.

estimates of rate constants that are unavailable for medium-sized Criegee intermediates.

The present paper sets out a roadmap for computationally feasible and accurate calculation of related reactions. It is only very recently that these reactions became directly accessible experimentally, and tropospherically relevant ranges of temperature are still experimentally difficult. Theory at the level described here can provide more accurate values than current experiments. Additionally, theoretical methods can also predict products, which often determine the tropospheric importance of these reactions and which are not often measured experimentally.

Structure of $(CH_3)_2COO$

The structure of $(CH_3)_2COO$ has been experimentally measured using both Fourier transform microwave spectroscopy (53) and UV absorption spectroscopy (54). We calculated the rotational constant of the equilibrium structure of $(CH_3)_2COO$ using CCSD(T)-F12a/DZ-F12, QCISD/TZ, MN15-L/MG3S, and MN15-L/mTZ, and *SI Appendix*, Table S3 shows that the maximum deviation from the experimental values is only 43 MHz.

Unimolecular Reaction of $(CH_3)_2COO$

There are two unimolecular reactions (with transition states **Uhs**-TS and **Uc**-TS) in Fig. 1. Fig. 1 and Table 2 show that the dominant unimolecular reaction is the hydrogen shift **Uhs** from CH_3 to the terminal oxygen atom.

Our best estimate of $\Delta H_0^{\ddagger}$ [calculated by W3X-L//CCSD(T)-F12a/DZ-F12] is given in Table 2 and is 16.37 kcal/mol. More details are in *SI Appendix*. Table 2 shows that the enthalpy of activation of **Uhs** at 0 K is estimated to be 15.92 kcal/mol by W2X and 15.91 by the larger-basis set MW2-F12 method; the good agreement of these values indicates that they are close to the CCSD(T)/CBS limit. They also agree well with the value of 16.06 kcal/mol calculated (37) by QCISD(T)/CBS//B3LYP/6–311 + G(2d,2p) including core correlation. However, the result with W3X-L, which is an approximation to CCSDT(Q)/CBS, differs from the W2X value by 0.45 kcal/mol, and this shows that one must go beyond CCSD(T).

Table 2 shows that MN15-L/mTZ gives an enthalpy of activation of 16.08 kcal/mol, which is more accurate than the CCSD(T)/CBS limit. Therefore, MN15-L/mTZ is chosen to do direct dynamics calculations for **Uhs**-TS in the unimolecular reaction of $(CH_3)_2COO$.

The Bimolecular Reaction of $(CH_3)_2COO$ with H_2O

There are four pathways for the $(CH_3)_2COO + H_2O$ reaction; these are shown in Fig. 1, where they correspond to two different reaction mechanisms: addition-coupled hydrogen transfer (**Ba**-TS1 and **Ba**-TS2) and double hydrogen atom transfer (**Bdhs**-TS1 and **Bdhs**-TS2) similar to the reaction of *syn*-$CH_3CHOO + H_2O$ reaction (41). Our best estimates of the enthalpies of activation at 0 K for the two pathways of **Ba** are calculated to be 5.89 and 6.97 kcal/mol (Table 2), which are different by ∼2 kcal/mol to 3 kcal/mol from previous investigations (39, 40); such deviations can lead to orders of magnitude differences in rate constants at atmospheric temperatures. Furthermore, note that the enthalpies of activation at 0 K for **Ba**-TS1 and **Ba**-TS2 are increased to 0.47 and 0.48 kcal/mol, respectively, when the post-CCSD(T) calculations are used (compare W2X and W3X-L in Table 2); this shows that post-CCSD(T) calculations are also required to obtain quantitative results in the $(CH_3)_2COO + H_2O$ reaction.

Since the enthalpies of Ba-TS1 and **Ba**-TS2 differ by only ∼1 kcal/mol, both can contribute to the rate. The enthalpies of activation at 0 K for **Ba**-TS1 and **Ba**-TS2 calculated by M11-L/MG3S are estimated to be 6.10 and 7.24 kcal/mol (bold in Table 2), which differ from the best estimates by only 0.21 kcal/mol to 0.27 kcal/mol; this shows that M11-L/MG3S exceeds CCSD(T)/CBS accuracy for the addition-coupled hydrogen transfer in the $(CH_3)_2COO + H_2O$ reaction. Thus, M11-L/MG3S has been chosen to do direct dynamics calculations for **Ba**.

The double hydrogen atom transfer processes occur via the transition states **Bdhs**-TS1 and **Bdhs**-TS2, where water acts as a catalyst. Table 2 shows $\Delta H_0^{\ddagger}$ best estimates of 8.87 and 8.82 kcal/mol. Although these are ∼0.9 kcal/mol to 1 kcal/mol lower than those of the double hydrogen atom transfer for the *syn*-$CH_3CHOO + H_2O$ reaction (41), they are too high to allow this reaction to compete significantly with **Ba**. Table 2 also tells us that the enthalpies of activation for **Bdhs**-TS1 and **Bdhs**-TS2 at 0 K calculated by M11-L/MG3S are 7.84 and 7.80 kcal/mol, which are about 1 kcal/mol lower than those of our best estimates. However, our dual-level calculation of the rate constant should

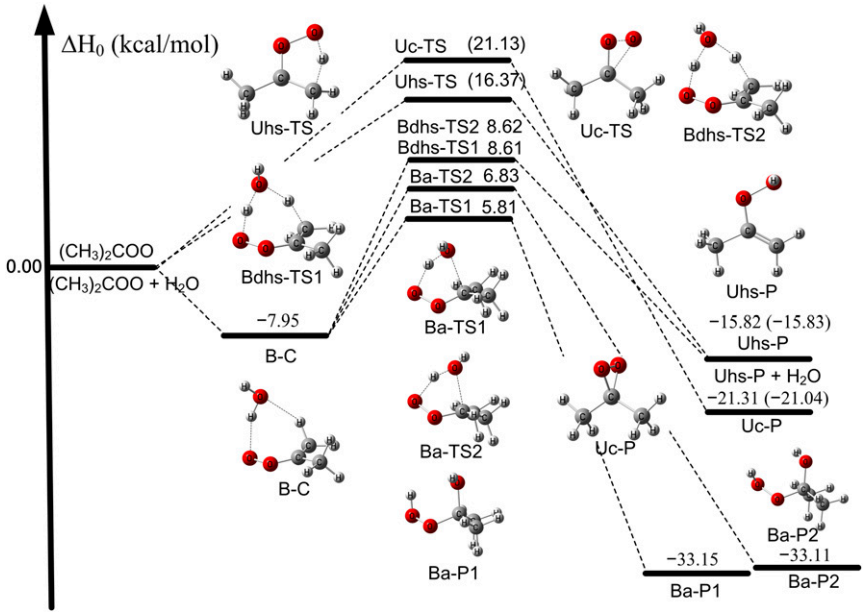

Fig. 1. The calculated enthalpy profile by the W3X//QCISD/TZ [for a few structures, we also give the W3X-L//CCSD(T)-F12a/DZ-F12 result in parentheses].

Table 2. Enthalpies of activation at 0 K ($\Delta H_0^{\ddagger}$, in kcal/mol)

Methods	Ba-TS1	Ba-TS2	Bdhs-TS1	Bdhs-TS2	Uhs-TS	Uc-TS
W3X-L//CCSD(T)-F12a/DZ-F12	5.89	6.97	8.87	8.82	16.37	21.13
W3X//QCISD/TZ	5.81	6.83	8.61	8.62	15.91	20.92
MW2-F12//CCSD(T)-F12a/DZ-F12					15.92	
W2X//CCSD(T)-F12a/DZ-F12	5.42	6.49	8.40	8.35	15.92	21.42
CCSD(T)-F12a/DZ-F12	5.39	6.45	8.70	8.65	16.05	21.18
MN15-L/mTZ	7.04	8.12	10.90	10.80	**16.08**	**21.00**
M11-L/MG3S	**6.10**	**7.24**	**7.84**	**7.80**	13.97	22.18
MN15-L/MG3S	7.48	8.65	11.64	11.58	16.73	21.34
M11-L/mTZ	6.14	7.11	7.72	7.67	13.34	21.43

The top row contains the most accurate calculations (benchmarks); the values in bold are those used in direct dynamics calculations.

be adequate to cancel most of this error, since this is the smaller component of the bimolecular reaction rate.

Calculated Rate Constants

As shown in *SI Appendix*, Table S7, the pressure dependence of the unimolecular reaction is not significant under the conditions of interest here, and as discussed in *SI Appendix*, in the section on low-pressure rate constants on p. S-12, the bimolecular rate constant is also not expected to depend significantly on pressure, and so, in the article proper, we limit consideration to the high-pressure limiting rate constants for these reactions. These rate constants are provided in *SI Appendix*, Table S5, as calculated using multi-structural variational transition state theory with the SCT approximation for tunneling. The bimolecular rate constant $k_{\mathbf{B}}$ and the unimolecular rate constant $k_{\mathbf{U}}$ are fitted as

$$k_{\mathbf{B}} = 3.0668\times10^{-11}\left(\frac{\mathrm{T}+239.53642}{300}\right)^{-5.46455}\exp\left[-\frac{6.28796(T+\ 239.53642)}{R(T^2+57377.69651)}\right] \quad [1]$$

$$k_{\mathbf{U}} = 5.9458\times10^{-4}\left(\frac{\mathrm{T}+88.31431}{300}\right)^{27.57662}\exp\left[-\frac{-3.22616(T+88.31431)}{R(T^2+7799.417351)}\right], \quad [2]$$

where the functional form is that suggested previously (55). The temperature-dependent Arrhenius activation energy was computed from the fit as (56)

$$E_a = -R\frac{d\ \ln k}{d(1/T)}. \quad [3]$$

The bimolecular rate constant is calculated to have an activation energy that decreases from 2.8 kcal/mol at 298 K to 0.9 kcal/mol at 190 K. The activation energy for unimolecular hydrogen shift reaction depends more strongly on temperature; it decreases from 8.5 kcal/mol at 298 K to 3.4 kcal/mol at 190 K. Full table of $E_a(T)$ are in *SI Appendix*, Table S5. A temperature-dependent activation energy corresponds to a nonlinear Arrhenius plot, which makes it very hard to extrapolate experimental results.

The unimolecular rate constant for **Uhs** is computed to be 749 s^{-1} at 310 K, which is in good agreement with the experimental value (628 ± 60 s^{-1}) at 310 K (35). However, our calculated value (1,380 s^{-1}) is slightly higher than that of the experimental value (916 ± 56 s^{-1}) at 323 K and between 100 Torr and 200 Torr (34). The calculated rate constants at lower temperatures are 202, 329, and 420 s^{-1} at 283, 293, and 298 K, respectively, and these are in excellent agreement with the directly measured experimental values of 269 ± 82, 305 ± 70, and 361 ± 49 s^{-1} (34, 35), but the calculations provide results down to lower temperatures as well, which is very important for modeling since, as discussed in the previous paragraph, the Arrhenius plot is very nonlinear.

The computed rate constant of the bimolecular reaction is 1.12×10^{-17} cm^3 per molecule per second at 298 K, which does not exceed the experimental upper limit of 1.5×10^{-16} cm^3 per molecule per second (22). We find that the double transfer process accounts for only 11 to 17% of the overall $(CH_3)_2COO + H_2O$ reaction rate at 190 K to 350 K (*SI Appendix*, Table S5); this finding is different from what was seen for the *syn*-$CH_3CHOO + H_2O$

Table 3. Calculated atmospheric lifetimes (in milliseconds) of bimolecular reaction of $(CH_3)_2COO$ with H_2O (τ_B), its unimolecular reaction (τ_U), and its bimolecular reaction with SO_2 (τ_{SO2})

		τ_B	τ_{SO2}		
T/K	τ_U	$[H_2O] = 3.8\times10^{17}$	$[SO_2] = 9\times10^{9}$	$[SO_2] = 5\times10^{11}$	$[SO_2] = 1\times10^{12}$
200	278	651	59	11	5
220	106	475	65	12	6
230	66	401	68	12	6
240	40	339	71	13	6
250	25	287	73	13	7
260	15	243	76	14	7
270	9.3	206	78	14	7
280	5.7	175	80	14	7
290	3.5	149	83	15	7
298	2.4	132	85	15	8

Concentrations are in brackets and are in molecules per cubic centimeter. The lifetime for unimolecular reaction with rate constant k is $1/k$. The lifetime for bimolecular reaction with X is $\tau = 1/[X]k_X$, where k_X is the bimolecular rate constant for reaction with X.

reaction, where the double hydrogen transfer process was found to dominate below 290 K (41). The difference is mainly due to tunneling as shown by *SI Appendix*, Table S6. For example, tunneling increases the rate constant through **Ba**-TS1 by a factor of 490 at 190 K and by a factor of 11.2 at 298 K; tunneling is even more importance for **Ba**-TS2.

Atmospheric Implications

The competition between unimolecular reaction of $(CH_3)_2COO$ and its bimolecular reactions with H_2O and SO_2 at different altitudes (and hence different temperatures) is important because Criegee intermediates are potential oxidizers of SO_2 to SO_3 (3). The atmospheric lifetimes of Criegee intermediates depend on the rate constants of its unimolecular reactions and the bimolecular reaction with atmospheric molecules combined with the corresponding concentrations of these atmospheric molecules. The concentrations vary by altitude, latitude, humidity, distance from sources of SO_2, and other variables. For the unimolecular reaction and reaction with H_2O, we use the rate constants calculated in the present work. The rate constants of the $(CH_3)_2COO + SO_2$ reaction are not known experimentally over the whole atmospheric temperature range; however, experiments have yielded 1.3×10^{-10} cm^3 per molecule per second at 298 K (20). To estimate the temperature dependence, we investigated the simpler reaction of CH_2OO with SO_2 and used its temperature dependence to estimate the temperature dependence of $(CH_3)_2COO + SO_2$ (see *SI Appendix*, pp. S-12; see Table S8), and this estimate will be used here. Based on these rate constants, Table 3 gives the lifetimes for selected possible concentrations of H_2O and SO_2; additional results and background data are given in *SI Appendix*. Table 3 and *SI Appendix*, Table S9 show that, for SO_2 concentrations of 9×10^{10} (9), 5×10^{11}, and 1×10^{12} molecules per cubic centimeter, the $(CH_3)_2COO + SO_2$ reaction dominates the removal of $(CH_3)_2COO$ below 240, 260, and 270 K, respectively.

Summary

We used CCSDT(Q)/CBS (obtained by extrapolation) enthalpies of activation to select and validate exchange-correlation functionals, which, in turn, were used to calculate rate constants of the unimolecular reaction of $(CH_3)_2COO$ and the bimolecular reaction with water, with accuracy comparable to experiments but covering the full range of tropospheric temperature and pressure. These rate constants can be used to estimate the atmospheric lifetimes for specific reactions, and they show how theoretical methods can predict reliable rate constants for atmospheric modeling.

Computational Details

We summarize the methods here; full details are in *SI Appendix*. Benchmark calculations were executed using W3X-L//CCSD(T)-F12a/DZ-F12 theoretical method for transition states in the unimolecular reaction of $(CH_3)_2COO$ and its reaction with H_2O. W3X-L has been used to obtain single-point energies close to CCSDT(Q)/CBS in the small Criegee intermediates + H_2O (41) SO_2 + OH (57), HO_2 + FCHO (58), and $CH_3O + H_2O$ (59) reactions. In addition, W3X/QCISD/TZ was used to reevaluate the energetics of the unimolecular reaction of $(CH_3)_2COO$ and its reaction with H_2O to determine the reliability of this method compared with W3X-L//CCSD(T)-F12a/DZ-F12 results. These high-level theoretical results were used to validate the MN15-L/mTZ and M11-L/MG3S density functionals for direct dynamics calculations, which were carried out for the unimolecular reaction of $(CH_3)_2COO$ and its bimolecular reaction with H_2O using multistructural variational transition state theory with small-curvature tunneling. A dual-level strategy (41, 60) (details are in *SI Appendix*) was used to correct the density functional rate constants for the difference in barrier heights of the benchmarks and the chosen functional. Scale factors (49) provided in *SI Appendix*, Table S2 were used in the thermochemistry and kinetics calculations to correct anharmonicity and systematic errors in high frequencies. In addition, we computed the torsional anharmonicity and torsion–rotation coupling (47, 48). Pressure-dependent rate constants for the unimolecular reaction were computed by system-specific quantum Rice–Ramsperger–Kassel theory with a thermal activation mechanism (61–63).

ACKNOWLEDGMENTS. We thank Prof. Kirk A. Peterson from Washington State University for information about CCSD(T)-F12b/cc-pV5Z-F12 calculations and Prof. Jan M. L. Martin from Weizmann Institute of Science for helpful discussion of MW2-F12 extrapolation. This work was supported in part by the US Department of Energy, Office of Science, Office of Basic Energy Sciences, Division of Chemical Sciences, Geosciences, and Biosciences under Contracts DE-AC02-06CH11357 and DE-SC0015997; in part by the National Natural Science Foundation of China Grant 41775125; and by the Science and Technology Foundation of Guizhou Province, China Grants [2015]350 and [2018]1080. Computations were performed using resources of Minnesota Supercomputing Institute and the National Energy Research Scientific Computing Center.

1. Criegee R (1975) Mechanism of ozonolysis. *Angew Chem Int Ed Engl* 14:745–752.
2. Johnson D, Marston G (2008) The gas-phase ozonolysis of unsaturated volatile organic compounds in the troposphere. *Chem Soc Rev* 37:699–716.
3. Mauldin RL, 3rd, et al. (2012) A new atmospherically relevant oxidant of sulphur dioxide. *Nature* 488:193–196.
4. Ziemann PJ, Atkinson R (2012) Kinetics, products, and mechanisms of secondary organic aerosol formation. *Chem Soc Rev* 41:6582–6605.
5. Ehn M, et al. (2014) A large source of low-volatility secondary organic aerosol. *Nature* 506:476–479.
6. Tröstl J, et al. (2016) The role of low-volatility organic compounds in initial particle growth in the atmosphere. *Nature* 533:527–531.
7. Taatjes CA (2017) Criegee intermediates: What direct production and detection can teach us about reactions of carbonyl oxides. *Annu Rev Phys Chem* 68:183–207.
8. Welz O, et al. (2012) Direct kinetic measurements of Criegee intermediate (CH_2OO) formed by reaction of CH_2I with O_2. *Science* 335:204–207.
9. Vereecken L, Harder H, Novelli A (2012) The reaction of Criegee intermediates with NO, RO_2, and SO_2, and their fate in the atmosphere. *Phys Chem Chem Phys* 14:14682–14695.
10. Chao W, Hsieh J-T, Chang C-H, Lin JJ-M (2015) Atmospheric chemistry. Direct kinetic measurement of the reaction of the simplest Criegee intermediate with water vapor. *Science* 347:751–754.
11. Long B, Cheng J-R, Tan X-F, Zhang W-J (2009) Theoretical study on the detailed reaction mechanisms of carbonyl oxide with formic acid. *J Mol Struct THEOCHEM* 916:159–167.
12. Long B, et al. (2011) Theoretical studies on reactions of the stabilized H_2COO with HO_2 and the $HO_2\cdots H_2O$ complex. *J Phys Chem A* 115:6559–6567.
13. Berndt T, et al. (2012) Gas-phase ozonolysis of selected olefins: The yield of stabilized Criegee intermediate and the reactivity toward SO_2. *J Phys Chem Lett* 3:2892–2896.
14. Jalan A, Allen JW, Green WH (2013) Chemically activated formation of organic acids in reactions of the Criegee intermediate with aldehydes and ketones. *Phys Chem Chem Phys* 15:16841–16852.
15. Berndt T, et al. (2014) H_2SO_4 formation from the gas-phase reaction of stabilized Criegee intermediates with SO_2: Influence of water vapour content and temperature. *Atmos Environ* 89:603–612.
16. Buras ZJ, Elsamra RMI, Green WH (2014) Direct determination of the simplest Criegee intermediate (CH_2OO) self reaction rate. *J Phys Chem Lett* 5:2224–2228.
17. Su Y-T, et al. (2014) Extremely rapid self-reaction of the simplest Criegee intermediate CH_2OO and its implications in atmospheric chemistry. *Nat Chem* 6:477–483.
18. Berndt T, et al. (2014) Competing atmospheric reactions of CH_2OO with SO_2 and water vapour. *Phys Chem Chem Phys* 16:19130–19136.
19. Vereecken L, Glowacki DR, Pilling MJ (2015) Theoretical chemical kinetics in tropospheric chemistry: Methodologies and applications. *Chem Rev* 115:4063–4114.
20. Osborn DL, Taatjes CA (2015) The physical chemistry of Criegee intermediates in the gas phase. *Int Rev Phys Chem* 34:309–360.
21. Kuwata KT, et al. (2015) A computational re-examination of the Criegee intermediate–sulfur dioxide reaction. *J Phys Chem A* 119:10316–10335.
22. Huang H-L, Chao W, Lin JJ-M (2015) Kinetics of a Criegee intermediate that would survive high humidity and may oxidize atmospheric SO_2. *Proc Natl Acad Sci USA* 112:10857–10862.
23. Elsamra RMI, Jalan A, Buras ZJ, Middaugh JE, Green WH (2016) Temperature- and pressure-dependent kinetics of $CH_2OO + CH_3COCH_3$ and $CH_2OO + CH_3CHO$: Direct measurements and theoretical analysis. *Int J Chem Kinet* 48:474–488.
24. Smith MC, et al. (2017) Temperature-dependent rate coefficients for the reaction of CH_2OO with hydrogen sulfide. *J Phys Chem A* 121:938–945.
25. Raghunath P, Lee Y-P, Lin MC (2017) Computational chemical kinetics for the reaction of Criegee intermediate CH_2OO with HNO_3 and its catalytic conversion to OH and HCO. *J Phys Chem A* 121:3871–3878.

26. Kumar M, Francisco JS (2017) Reactions of Criegee intermediates with non-water greenhouse gases: Implications for metal free chemical fixation of carbon dioxide. *J Phys Chem Lett* 8:4206–4213.
27. Liu Y, et al. (2017) A kinetic study of the CH_2OO Criegee intermediate reaction with SO_2, $(H_2O)_2$, CH_2I_2 and I atoms using OH laser induced fluorescence. *Phys Chem Chem Phys* 19:20786–20794.
28. Lee Y-P (2015) Perspective: Spectroscopy and kinetics of small gaseous Criegee intermediates. *J Chem Phys* 143:020901.
29. Kroll JH, Clarke JS, Donahue NM, Anderson JG (2001) Mechanism of HO_x formation in the gas-phase ozone–alkene reaction. 1. Direct, pressure-dependent measurements of prompt OH yields. *J Phys Chem A* 105:1554–1560.
30. Kroll JH, Sahay SR, Anderson JG, Demerjian KL, Donahue NM (2001) Mechanism of HO_x formation in the gas-phase ozone-alkene reaction. 2. Prompt versus thermal dissociation of carbonyl oxides to form OH. *J Phys Chem A* 105:4446–4457.
31. Campos-Pineda M, Zhang J (2017) Low-pressure yields of stabilized Criegee intermediates CH_3CHOO and $(CH_3)_2COO$ in ozonolysis of trans-2-butene and 2,3-dimethyl-2-butene. *Chem Phys Lett* 683:647–652.
32. Newland MJ, et al. (2015) Kinetics of stabilised Criegee intermediates derived from alkene ozonolysis: Reactions with SO_2, H_2O and decomposition under boundary layer conditions. *Phys Chem Chem Phys* 17:4076–4088.
33. Fang Y, et al. (2016) Communication: Real time observation of unimolecular decay of Criegee intermediates to OH radical products. *J Chem Phys* 144:061102.
34. Smith MC, Chao W, Takahashi K, Boering KA, Lin JJ-M (2016) Unimolecular decomposition rate of the Criegee intermediate $(CH_3)_2COO$ measured directly with UV absorption spectroscopy. *J Phys Chem A* 120:4789–4798.
35. Chhantyal-Pun R, et al. (2017) Direct measurements of unimolecular and bimolecular reaction kinetics of the Criegee intermediate $(CH_3)_2COO$. *J Phys Chem A* 121:4–15.
36. Drozd GT, Kurtén T, Donahue NM, Lester MI (2017) Unimolecular decay of the dimethyl-substituted Criegee intermediate in alkene ozonolysis: Decay time scales and the importance of tunneling. *J Phys Chem A* 121:6036–6045.
37. Yin C, Takahashi K (2017) How does substitution affect the unimolecular reaction rates of Criegee intermediates? *Phys Chem Chem Phys* 19:12075–12084.
38. Kuwata KT, et al. (2018) Quantum chemical and statistical rate theory studies of the vinyl hydroperoxides formed in trans-2-butene and 2,3-dimethyl-2-butene ozonolysis. *J Phys Chem A* 122:2485–2502.
39. Ryzhkov AB, Ariya PA (2004) A theoretical study of the reactions of parent and substituted Criegee intermediates with water and the water dimer. *Phys Chem Chem Phys* 6:5042–5050.
40. Anglada JM, González J, Torrent-Sucarrat M (2011) Effects of the substituents on the reactivity of carbonyl oxides. A theoretical study on the reaction of substituted carbonyl oxides with water. *Phys Chem Chem Phys* 13:13034–13045.
41. Long B, Bao JL, Truhlar DG (2016) Atmospheric chemistry of Criegee intermediates: Unimolecular reactions and reactions with water. *J Am Chem Soc* 138:14409–14422.
42. Chan B, Radom L (2015) W2X and W3X-L: Cost-effective approximations to W2 and W4 with kJ $mol^{(-1)}$ accuracy. *J Chem Theory Comput* 11:2109–2119.
43. Garrett BC, Truhlar DG (1979) Criterion of minimum state density in the transition state theory of bimolecular reactions. *J Chem Phys* 70:1593–1598.
44. Liu Y-P, et al. (1993) Molecular modeling of the kinetic isotope effect for the [1,5]-sigmatropic rearrangement of *cis*-1,3-pentadiene. *J Am Chem Soc* 115:2408–2415.
45. Liu Y-P, Lu D-h, Gonzàlez-Lafont A, Truhlar DG, Garrett BC (1993) Direct dynamics calculation of the kinetic isotope effect for an organic hydrogen-transfer reaction, including corner-cutting tunneling in 21 dimensions. *J Am Chem Soc* 115:7806–7817.
46. Yu T, Zheng J, Truhlar DG (2011) Multi-structural variational transition state theory. Kinetics of the 1,4-hydrogen shift isomerization of the pentyl radical with torsional anharmonicity. *Chem Sci (Camb)* 2:2199–2213.
47. Zheng J, et al. (2011) Practical methods for including torsional anharmonicity in thermochemical calculations on complex molecules: The internal-coordinate multi-structural approximation. *Phys Chem Chem Phys* 13:10885–10907.
48. Zheng J, Truhlar DG (2013) Quantum thermochemistry: Multistructural method with torsional anharmonicity based on a coupled torsional potential. *J Chem Theory Comput* 9:1356–1367.
49. Alecu IM, Zheng J, Zhao Y, Truhlar DG (2010) Computational thermochemistry: Scale factor databases and scale factors for vibrational frequencies obtained from electronic model chemistries. *J Chem Theory Comput* 6:2872–2887.
50. Allison TC, Truhlar DG (1998) Testing the accuracy of practical semiclassical methods: Variational transition state theory with optimized multidimensional tunneling. *Modern Methods for Multidimensional Dynamics Computations in Chemistry*, ed Thompson DL (World Sci, Singapore), pp 618–712.
51. Truhlar DG, Garrett BC (2007) Variational transition state theory in the treatment of hydrogen transfer reactions. *Hydrogen-Transfer Reactions*, eds Hynes JT, Klinman JP, Limbach H-H, Schowen RL (Wiley-VCH, Weinheim, Germany), Vol 2, pp 833–874.
52. Bao JL, Truhlar DG (2017) Variational transition state theory: Theoretical framework and recent developments. *Chem Soc Rev* 46:7548–7596.
53. Nakajima M, Endo Y (2016) Fourier-transform microwave spectroscopy of dimethyl-substituted Criegee intermediate $(CH_3)_2COO$. *J Chem Phys* 145:244307.
54. Chang Y-P, Chang C-H, Takahashi K, Lin JJ-M (2016) Absolute UV absorption cross sections of dimethyl substituted Criegee intermediate $(CH_3)_2COO$. *Chem Phys Lett* 653:155–160.
55. Zheng J, Truhlar DG (2010) Kinetics of hydrogen-transfer isomerizations of butoxyl radicals. *Phys Chem Chem Phys* 12:7782–7793.
56. Truhlar DG (1978) Interpretation of activation energy. *J Chem Educ* 55:309–311.
57. Long B, Bao JL, Truhlar DG (2017) Reaction of SO_2 with OH in the atmosphere. *Phys Chem Chem Phys* 19:8091–8100.
58. Long B, Tan X-F, Bao JL, Wang D-M, Long Z-W (2017) Theoretical study of the reaction mechanism and kinetics of HO_2 with XCHO (X = F, Cl). *Int J Chem Kinet* 49:130–139.
59. Wei M-L, Tan X-F, Long Z-W, Long B (2017) Atmospheric chemistry of CH_3O: Its unimolecular reaction and reactions with H_2O, NH_3, and HF. *RSC Adv* 7:56211–56219.
60. Tan XF, et al. (2018) Atmospheric chemistry of CH_3CHO: The hydrolysis of CH_3CHO catalyzed by H_2SO_4. *Phys Chem Chem Phys* 20:7701–7709.
61. Bao JL, Zheng J, Truhlar DG (2016) Kinetics of hydrogen radical reactions with toluene including chemical activation theory employing system-specific quantum RRK theory calibrated by variational transition state theory. *J Am Chem Soc* 138:2690–2704.
62. Bao JL, Truhlar DG (2016) Silane-initiated nucleation in chemically active plasmas: Validation of density functionals, mechanisms, and pressure-dependent variational transition state calculations. *Phys Chem Chem Phys* 18:10097–10108.
63. Bao JL, Zhang X, Truhlar DG (2016) Predicting pressure-dependent unimolecular rate constants using variational transition state theory with multidimensional tunneling combined with system-specific quantum RRK theory: A definitive test for fluoroform dissociation. *Phys Chem Chem Phys* 18:16659–16670.
64. Pople JA, Head-Gordon M, Raghavachari K (1987) Quadratic configuration interaction. A general technique for determining electron correlation energies. *J Chem Phys* 87:5968–5975.
65. Raghavachari K, Trucks GW, Pople JA, Head-Gordon M (1989) A fifth-order perturbation comparison of electron correlation theories. *Chem Phys Lett* 157:479–483.
66. Knizia G, Adler TB, Werner H-J (2009) Simplified CCSD(T)-F12 methods: Theory and benchmarks. *J Chem Phys* 130:054104.
67. Bomble YJ, Stanton JF, Kállay M, Gauss J (2005) Coupled-cluster methods including noniterative corrections for quadruple excitations. *J Chem Phys* 123:054101.
68. Sylvetsky N, Peterson KA, Karton A, Martin JML (2016) Toward a W4-F12 approach: Can explicitly correlated and orbital-based ab initio CCSD(T) limits be reconciled? *J Chem Phys* 144:214101.
69. Chan B, Radom L (2013) W3X: A cost-effective post-CCSD(T) composite procedure. *J Chem Theory Comput* 9:4769–4778.
70. Stephens PJ, Devlin FJ, Chabalowski CF, Frisch MJ (1994) Ab initio calculation of vibrational absorption and circular dichroism spectra using density functional force fields. *J Phys Chem* 98:11623–11627.
71. Peverati R, Truhlar DG (2012) M11-L: A local density functional that provides improved accuracy for electronic structure calculations in chemistry and physics. *J Phys Chem Lett* 3:117–124.
72. Yu HS, He X, Truhlar DG (2016) MN15-L: A new local exchange-correlation functional for Kohn–Sham density functional theory with broad accuracy for atoms, molecules, and solids. *J Chem Theory Comput* 12:1280–1293.
73. Frisch MJ, Pople JA, Binkley JS (1984) Self-consistent molecular orbital methods 25. Supplementary functions for Gaussian basis sets. *J Chem Phys* 80:3265–3269.
74. Lynch BJ, Zhao Y, Truhlar DG (2003) Effectiveness of diffuse basis functions for calculating relative energies by density functional theory. *J Phys Chem A* 107:1384–1388.
75. Peterson KA, Adler TB, Werner H-J (2008) Systematically convergent basis sets for explicitly correlated wavefunctions: The atoms H, He, B-Ne, and Al-Ar. *J Chem Phys* 128:084102.
76. Dunning TH, Jr (1989) Gaussian basis sets for use in correlated molecular calculations. I. The atoms boron through neon and hydrogen. *J Chem Phys* 90:1007–1023.
77. Papajak E, Leverentz HR, Zheng J, Truhlar DG (2009) Efficient diffuse basis sets: cc-pVxZ+ and maug-cc-pVxZ. *J Chem Theory Comput* 5:1197–1202.
78. Kendall RA, Dunning TH, Jr, Harrison RJ (1992) Electron affinities of the first-row atoms revisited. Systematic basis sets and wave functions. *J Chem Phys* 96:6796–6806.
79. Halkier A, et al. (1998) Basis-set convergence in correlated calculations on Ne, N_2, and H_2O. *Chem Phys Lett* 286:243–252.
80. Garrett BC, Truhlar DG (1979) Semiclassical tunneling calculations. *J Phys Chem* 83: 2921–2926.